

## Damage to the Surface Layer of Inconel 718 Alloy by Pulsed Beam-Plasma Flows

I. V. Borovitskaya<sup>a, \*</sup>, A. S. Demin<sup>a</sup>, O. A. Komolova<sup>a</sup>, S. V. Latyshev<sup>a, b</sup>, S. A. Maslyaev<sup>a</sup>,  
I. S. Monakhov<sup>a, c</sup>, E. V. Morozov<sup>a</sup>, V. N. Pimenov<sup>a, \*\*</sup>, I. P. Sasinovskaya<sup>a</sup>, G. G. Bondarenko<sup>c</sup>,  
A. I. Gaydar<sup>d</sup>, and I. A. Logachev<sup>e</sup>

<sup>a</sup> *Baikov Institute of Metallurgy and Materials Science, Russian Academy of Sciences (IMET RAS), Moscow, 119334 Russia*

<sup>b</sup> *Moscow Technical University of Communications and Informatics (MTUCI), Moscow, 111024 Russia*

<sup>c</sup> *National Research University Higher School of Economics (HSE University), Moscow, 101000 Russia*

<sup>d</sup> *Scientific Research Institute of Advanced Materials and Technologies, Moscow, 115054 Russia*

<sup>e</sup> *National University of Science and Technology MISiS, Moscow, 119049 Russia*

\*e-mail: [symp@imet.ac.ru](mailto:symp@imet.ac.ru)

\*\*e-mail: [pimval@mail.ru](mailto:pimval@mail.ru)

Received October 5, 2022; revised December 26, 2022; accepted January 10, 2023

**Abstract**—Damage to the surface layer of the Inconel 718 alloy, manufactured by selective laser melting using additive technology followed by heat treatment, is studied under conditions of repeated pulsed exposure to flows of helium ions and helium plasma under two irradiation modes in the Vikhr Plasma Focus installation: in a soft mode with energy flux density  $q_0 = 2 \times 10^8$  W/cm<sup>2</sup> and pulse duration  $\tau = 50$  ns and in a hard mode with  $q_0 = 1.5 \times 10^9$  W/cm<sup>2</sup> and  $\tau = 25$  ns. The number of pulses in the experiments was  $N = 10$  and 20. Irradiation in a soft mode forms a microstructure containing pores on the layer surface, and with more severe energy exposure, surface microcracks and blisters with destroyed shells are formed. With an increase in the energy flux density, the surface layer erosion intensity (mass loss per pulse) increased. The nature of this phenomenon is determined by the processes of cleaning the surface layer of an alloy from impurity elements adsorbed from the external environment before irradiation, as well as the deposition of elements of functional materials and working gas impurities on the irradiated surface. Features of cellular microstructure formation of the surface layer (SL) of an alloy under study under the realized conditions of beam-plasma influences have been revealed. Using the numerical modeling method, the redistribution of the shares of energy absorbed by the material, spent on evaporation and melting of the irradiated surface layer (SL), in comparable irradiation modes was established.

**Keywords:** pulsed flows, helium plasma, helium ions, plasma focus, pores, blisters, microcracks, cellular microstructure

**DOI:** 10.1134/S2075113324700023

### INTRODUCTION

The issue of using high-nickel alloys as candidate materials for shells of fuel elements and covers of fuel assemblies of nuclear reactors is widely discussed by specialists [1–5].

The structural state and properties of Inconel 718 alloy are significantly influenced by its manufacturing technology. In particular, the introduction of powder modifiers in the form of titanium nitride or carbonitride nanoparticles into the melt helps to reduce the average grain sizes and increase the tensile strength at 650°C by 1.5–2 times [6]. Works [7–10] show that the introduction of rare earth metal atoms into the surface layers of heat-resistant nickel alloys using the ion

implantation method is a promising process that increases the performance characteristics of alloys.

In recent years, in many countries, including our country, additive technologies (AT) are used in the production of metal materials and products [11–15]. Manufacturing the Inconel 718 alloy by the AT method using layerwise laser melting (LLM) would make it possible to achieve mechanical strength in the finished product comparable to the strength of materials produced by traditional technologies [16]. The study of this alloy, melted by the direct laser growth (DLG) method according to the scheme of local supply of energy and powder material, revealed the peculiarities of the formation of its structural-phase state under the conditions of using the AT method [17].

Thus, the absence of the main strengthening components ( $\gamma'$  and  $\gamma''$  phases) and the low values of ultimate strength ( $\sigma_u$ ) and plastic limit ( $\sigma_p$ ) of a material in comparison with the standard technologies were noted in an alloy [17]. After heat treatment of an alloy obtained by the DLG method, the main strengthening phase is the  $\gamma'$  phase, and the impact strength increases by 1.5 times when changing the growth direction from longitudinal to transverse orientation relative to the dynamic effect on the material in the initial and heat-treated state [18].

In contrast to the well-studied physicochemical and mechanical properties of the Inconel 718 alloy, its radiation properties have not been sufficiently studied, in particular, regarding the resistance of a material to the effects of powerful pulsed radiation-thermal loads. In [19], the features of structural and phase changes in the surface layer (SL) of the Inconel 718 alloy under the influence of powerful pulsed flows of helium ions (HIs) and helium plasma (HP) in the irradiation mode below the melting threshold (MT) were studied. Surface melting occurred only in local micro regions owing to fluctuations in the incident energy flux, which led to the most noticeable structural changes.

The purpose of the work is to study the behavior of the Inconel 718 alloy, manufactured by selective laser melting (SLM) using an additive technology with subsequent heat treatment (hardening + aging), under repeated exposure to powerful pulsed beam-plasma flows.

## EXPERIMENTAL

For the experiments, the Inconel 718 alloy was chosen, prepared by the SLM method using powder material with a granulometric composition of  $<45 \mu\text{m}$ , which was obtained by plasma centrifugal spraying of a rod blank [19]. The chemical composition of Inconel 718 alloy was as follows in wt %: 50.0–55.0 Ni, 17.0–21.0 Cr, 4.75–5.5 Nb, 2.80–3.30 Mo, 0.65–1.15 Ti, 0.20–0.80 Al,  $<0.35$  Si,  $<0.08$  C,  $<0.3$  Cu, base Fe.

Samples of the alloy for irradiation with dimensions of  $12 \times 10 \times 1 \text{ mm}$  and  $10 \times 8 \times 1 \text{ mm}$  were cut from a disk with a diameter of 50 mm and placed in the cathode zone of the working chamber of the Vikhr Plasma Focus (PF) installation with an energy reserve in capacitors of  $\sim 2.1 \text{ kJ}$ . The sample irradiation scheme is shown in Fig. 1.

The mode of pulsed energy effects was chosen in such a way that the radiation flows incident on the target material generated nonequilibrium physical and chemical processes of an explosive nature (melting and high-speed crystallization, sputtering, evaporation, etc.) in the irradiated surface layer, affecting the

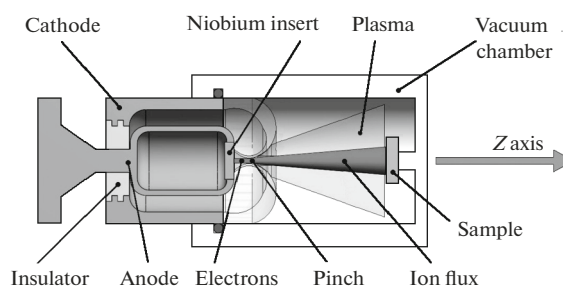


**Fig. 1.** Schematic diagram of irradiation of Inconel 718 alloy samples in the Vikhr Plasma Focus installation.

structural-phase and morphological characteristics of the alloy.

Samples were irradiated in a pulsed mode using helium as the working gas at a pressure in the chamber  $p_{\text{He}} \sim 300 \text{ Pa}$ . Target samples were placed normal to the incident energy flux at two different distances from the anode, providing soft (at  $L = 8 \text{ cm}$ ) or hard ( $L = 4 \text{ cm}$ ) irradiation modes. With each pulse discharge, the flows of helium ions and helium plasma acted on the target. The region of propagation of high-energy helium ions (with energy  $E \geq 100 \text{ keV}$ ) is limited by a conical surface with an apex angle (in the pinch zone—maximum plasma compression) of  $\sim 7\text{--}10^\circ$  [20]. Flows of helium ions (HIs) with lower energy propagate inside the cone with a larger angle at the apex of  $\sim 30^\circ$  (Fig. 1). The energy flux density incident on the target sample for the soft irradiation mode is  $q = 2 \times 10^8 \text{ W/cm}^2$  at a pulse duration of  $\tau = 50 \text{ ns}$ , and for the hard mode, it is  $q = 1.5 \times 10^9 \text{ W/cm}^2$  at  $\tau = 25 \text{ ns}$ . The number of pulse discharges for each irradiation mode was  $N = 10$  and  $N = 20$ .

The samples were weighed before and after irradiation on a VLR-200 analytical balance with an accuracy of  $e = 0.5 \text{ mg}$ .

Microstructure analysis of the samples was performed by optical microscopy (OM) on a Neophot-32 microscope and scanning electron microscopy (SEM) using a Zeiss EVO 40 scanning electron microscope.

The thermal effect of a beam of fast high-energy ions on the alloy under study was assessed by numerical simulation.

## RESULTS AND DISCUSSION

### *Surface Layer Microstructure*

Figures 2 and 3 show images of the alloy surface under study after it was irradiated in soft and hard modes. In both cases, the irradiation leads to melting of the surface layer and the formation of a wavelike relief, which is a set of waves (Figs. 2c, 3a, and 3c), the

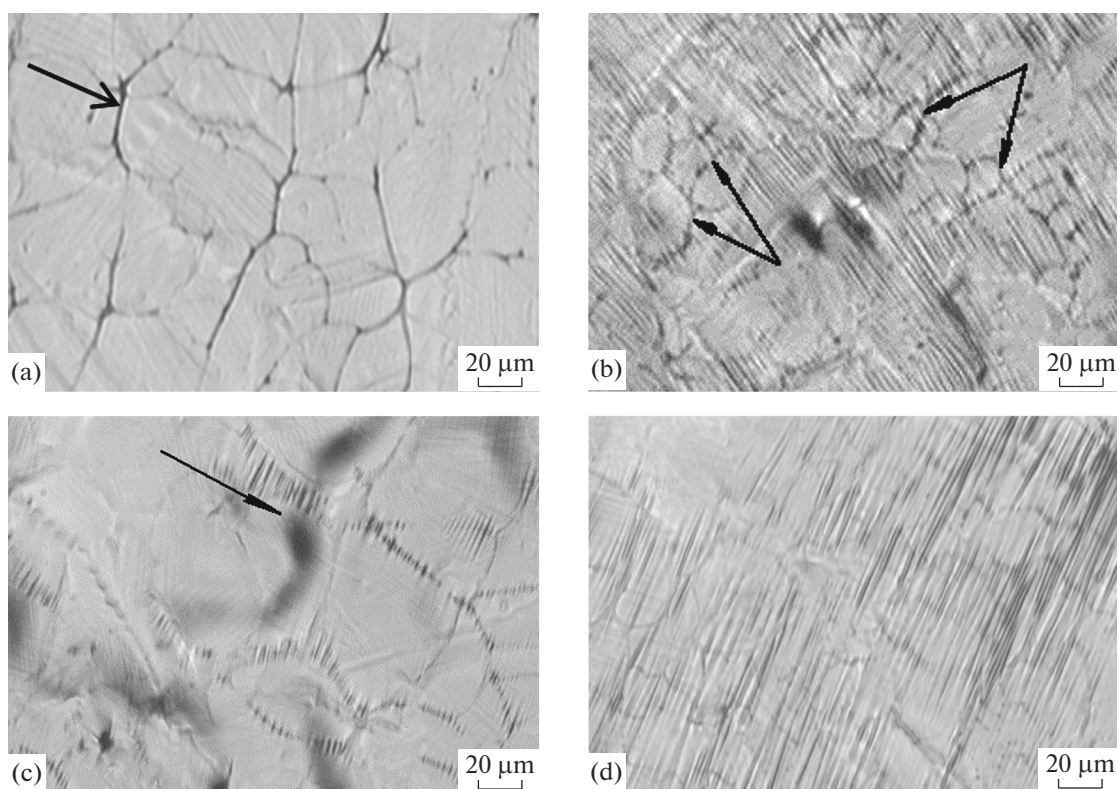


**Fig. 2.** Images of the surface of Inconel 718 alloy irradiated with fluxes of helium ions and helium plasma in a soft mode ( $q = 2 \times 10^8 \text{ W/cm}^2$ ,  $\tau = 50 \text{ ns}$ ): (a, b) at  $N = 10$ ; (c, d) at  $N = 20$ . Optical microscopy (OM).

height of which increases with an increase in radiation power density. In addition, the impact of helium ions (HIs) and helium plasma (HP) flows promotes the formation of a thin wrinkled film on the alloy surface, similar to ripples, which is observed in both irradiation modes. It is clearly visible in Figs. 2b and 3d. Its occurrence is apparently associated with the interaction of the components of the irradiated surface of the alloy with the residual impurity elements of the working gas (oxygen, nitrogen, carbon) at high temperatures. With an increase in the number of pulsed impacts, the total time of interaction of the elements of the alloy with the impurity elements of the working gas increases, which contributes to the formed film growth. In the soft irradiation mode, a microstructure is visible under the film (Figs. 2b and 3d), consisting of approximately equiaxed grains. Under harsh irradiation conditions, the “transparency effect” of a film is reduced, most likely because of its greater thickness; the grain character under the film is not observed, but a coarser microstructure in the form of waves is visible (Fig. 3d).

The nature of the microstructure under consideration can be traced in detail when analyzing the irradiated surface layer using the SEM method (Fig. 4). In the soft irradiation mode, in addition to the wavelike

relief (Figs. 4a, 4d, 4e) and the presence of a grain structure and surface film (Fig. 4b), slip lines are observed in some areas of the surface layer (Figs. 4c, 4f), indicating the occurrence of plastic deformation in it. In this case, in different areas of the irradiated surface, slip lines propagate along different slip systems [21]. One slip system is observed in some cases, and the slip lines in neighboring grains are located parallel or at an angle to each other (Fig. 5a). In other cases, the two slip systems are observed within individual grains (Fig. 5b).

The most intense plastic deformation occurred in the central zone of irradiation of an alloy, where there are areas with three systems of slip lines (Figs. 5c, 5d), which indicates the occurrence of plastic deformation under the action of tangential thermal stresses arising during cooling [22, 23] and dependence on orientation of microcrystallites relative to the direction of applied stress. On the basis of the concepts of [21], it can be assumed that, with different orientations of microcrystallites, the plastic deformation in some local sites proceeded according to the mechanism of sliding along planes (111) characteristic of metals with an fcc lattice (which includes the Inconel 718 alloy) with the participation of the most optimal sliding systems for



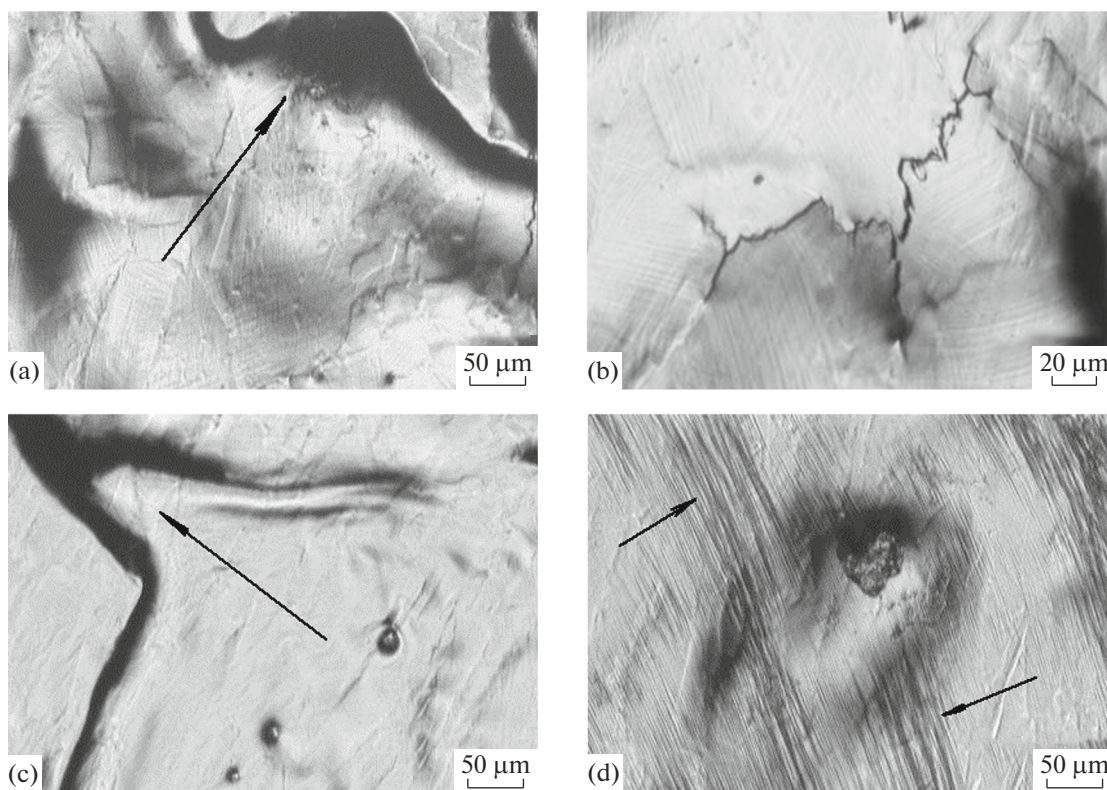


**Fig. 3.** Images of the surface of Inconel 718 alloy irradiated with fluxes of helium ions and helium plasma in a soft mode ( $q = 2 \times 10^9 \text{ W/cm}^2$ ,  $\tau = 25 \text{ ns}$ ): (a, b) at  $N = 10$ ; (c, d) at  $N = 20$ . Optical microscopy (OM).

this site. A similar situation occurred in ductile copper alloys with an fcc lattice of the Cu–Ni–Ga system when irradiated with deuterium ion fluxes and deuterium plasma [22].

Note also that, in the soft irradiation mode, pores appear on the surface of the alloy under study (Fig. 4d), through which the gas phase formed at high temperatures from helium ions implanted in the alloy and gas-forming impurity elements present in the alloy escaped from the melt.

In the hard regime of target irradiation, the blisters and microcracks are added to the already described signs of damage and structural changes on the surface (Figs. 6a, 6b). In addition, the cellular nature of the surface layer microstructure appears more clearly than in the soft mode (Figs. 6c, 6f). A similar nature of microstructure (cellular or cellular-dendritic type) was observed in other metallic materials after exposure to powerful beam-plasma flows. For example, in copper alloy Cu–4 wt % Ni–10 wt % Ga, such a microstructure appeared after irradiation with flows of deuterium plasma and deuterium ions under more severe conditions than in our case [22]. Zones of columnar crystals and a cellular microstructure of the surface with a cell size of  $\sim 100 \text{ nm}$  were also found in the irradiated

surface layer of niobium after exposure to pulsed helium ions (HIs) and helium plasma (HP) flows with a power density in the range of  $q = 10^7\text{--}10^8 \text{ W/cm}^2$  [23]. Specificity of the microstructure in the helium-irradiated Inconel 718 alloy is that it is not a zone of columnar crystals, but predominantly a set of parallel flat layers consisting of small cells with a size of  $\sim 200 \text{ nm}$  (Figs. 6c, 6f). In the direction normal to the irradiation plane, in some local regions, owing to temperature fluctuations arising as a result of inhomogeneity of the incident energy flux, columnar crystals can appear, which are formed during concentration supercooling in front of the directional crystallization front and were observed during irradiation of niobium (Fig. 7) under conditions similar to Inconel 718 alloy [23].

It is known that the material structure formation during crystallization depends on the ratio of the rates of nucleation and growth of crystals, which, in turn, are determined by the degree of supercooling of the melt. According to theory [24], at ultrahigh cooling rates of the melted surface layer (above  $10^6 \text{ K/s}$ ), a fine-cell structure is formed. A similar situation occurred in our case when irradiating the Inconel 718 alloy, since under the conditions of beam-plasma processing of samples the cooling rate of the molten sur-



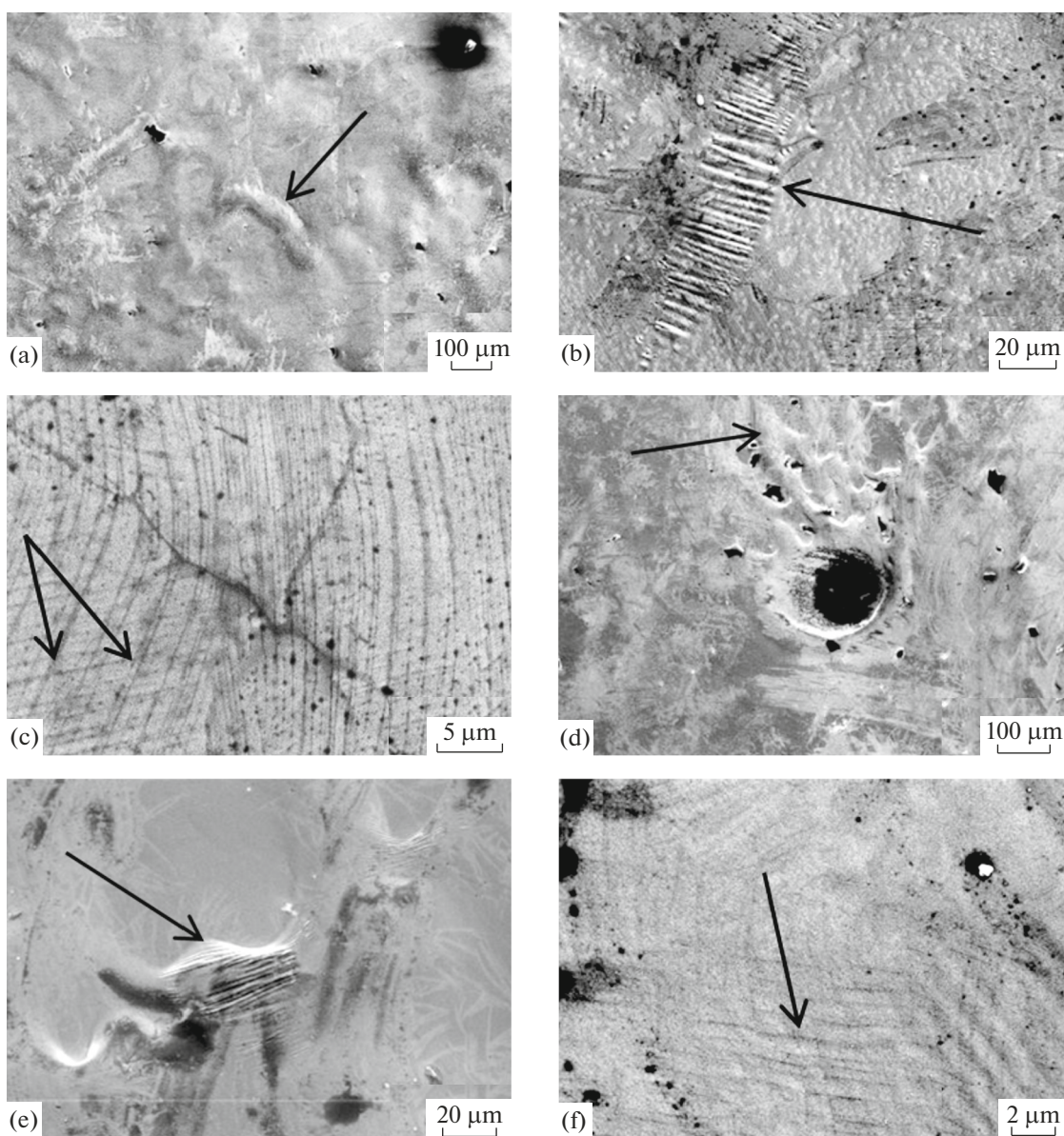


**Fig. 4.** SEM images of the surface of Inconel 718 alloy irradiated with fluxes of helium ions and helium plasma in a soft mode ( $q = 2 \times 10^8 \text{ W/cm}^2$ ,  $\tau = 50 \text{ ns}$ ) at  $N = 10$  (a, b, c) and  $N = 20$  (d, e, f).

face layer usually lies in the range of  $10^7$ – $10^9 \text{ K/s}$  [23, 25]. Note also that a similar fine-mesh microstructure was observed when the vanadium surface was irradiated in the Vikhr Plasma Focus installation with pulsed high-temperature nitrogen plasma [26].

#### *Surface Layer Erosion*

The degree of erosion of the alloy (mass loss due to a pulsed evaporation and sputtering) was determined by weighing the target sample before and after irradiation. The thickness of a layer  $h$  removed by the helium ions (HIs) and helium plasma (HP) flows in one pulse

(erosion rate) was approximately estimated using the formula

$$h = \frac{\Delta m}{\rho S N},$$

where  $\Delta m$  is the total mass loss of the sample during irradiation,  $\rho$  is the density of the alloy,  $S$  is the irradiation area, and  $N$  is the number of pulse impacts. The density value was taken from [27]. An analysis showed that, in the hard irradiation mode, the erosion rate  $h_2$  increases compared to the corresponding value  $h_1$  for the soft mode: at  $N = 10$ ,  $h_2/h_1 \sim 2$ , and at  $N = 20$ ,  $h_2/h_1 = 4$  (Table 1). In other words, the intensity of alloy erosion increases with an increase in the power

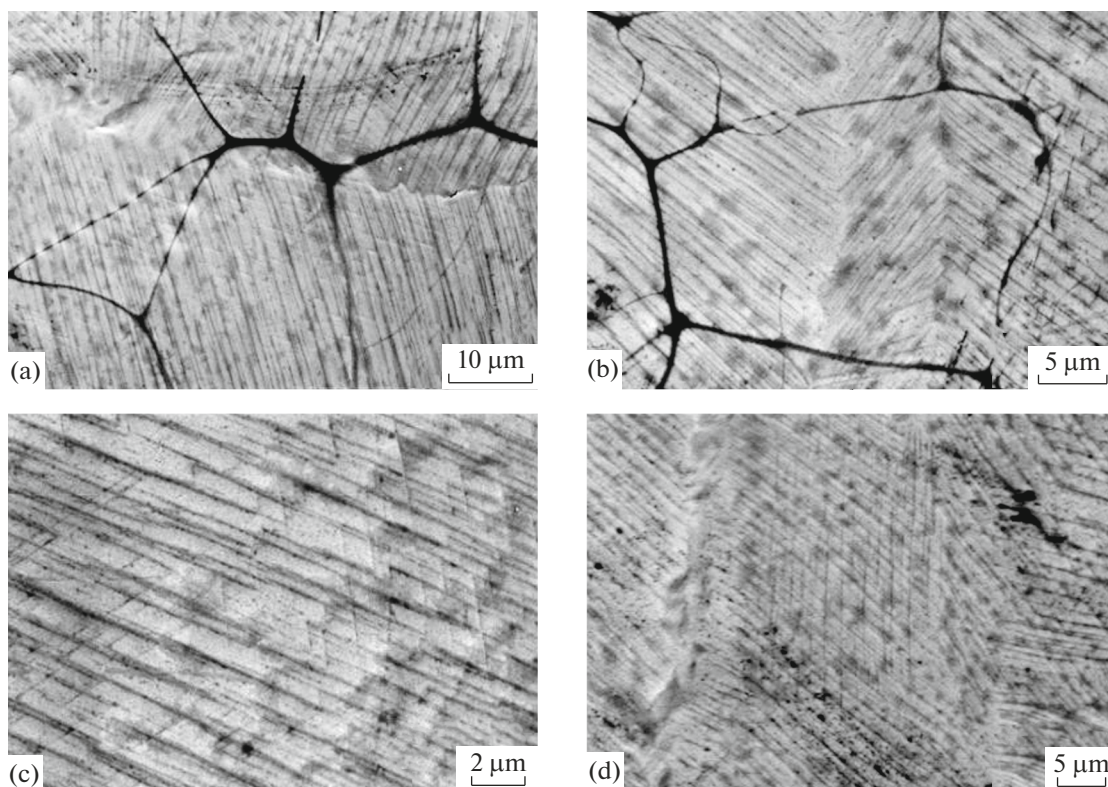


**Fig. 5.** SEM images of the surface of Inconel 718 alloy irradiated with fluxes of helium ions and helium plasma in a soft mode ( $q = 2 \times 10^8 \text{ W/cm}^2$ ,  $\tau = 50 \text{ ns}$ ) at  $N = 10$ , containing slip lines (a, b). (c, d) Areas of the central surface irradiation zone containing three slip systems.

density of radiation incident on the target sample. At the same time, within one irradiation mode, with an increase in  $N$ , a decrease in the value of  $h$  is observed: in the soft mode by about 3 times, in the hard mode by  $\sim 1.7$  times. This is due to the following factors. As  $N$  increases, as a rule, there is a gradual purification of the metal surface layer from impurity elements (O, N, C), which enter it before irradiation through absorption from the environment and during the preparation of polished samples for experiments. This fact, as shown in [23], helps reduce the erosion rate. Also,

with an increase in  $N$ , the mass of elements of the functional materials of the working chamber deposited on the irradiated surface of the alloy (in particular, the anode material [20, 23, 26]) increases, which leads to a decrease in the amount of mass loss  $\Delta m$ .

It should be noted that the observed erosion rate of the Inconel 718 alloy under the influence of helium ions (HIs) and helium plasma (HP) flows in the Vikhr Plasma Focus installation in the studied irradiation modes is slightly higher than that of W ( $h \approx 0.03 \mu\text{m/pulse}$ ) when irradiated in the Vikhr Plasma

**Table 1.** Erosion of Inconel 718 alloy during irradiation in the Vikhr PF installation

Irradiation mode	Sample number	Number of pulses, $N$	Sample mass before irradiation, $m_0$ , g	Sample mass after irradiation, $m$ , g	Mass loss, $\Delta m$ , g	1 Mass loss per pulse, $\Delta m/N$ , g	Evaporated layer thickness per pulse, $h$ , $\mu\text{m/pulse}$
1 (soft)	1	10	0.88775	0.88690	$8.5 \times 10^{-4}$	$8.5 \times 10^{-5}$	0.13
	2	20	1.48450	1.48370	$8.0 \times 10^{-4}$	$4.0 \times 10^{-5}$	0.04
2 (hard)	3	10	1.04125	1.03945	$18 \times 10^{-4}$	$1.8 \times 10^{-4}$	0.27
	4	20	1.53925	1.53615	$31 \times 10^{-4}$	$1.6 \times 10^{-4}$	0.16



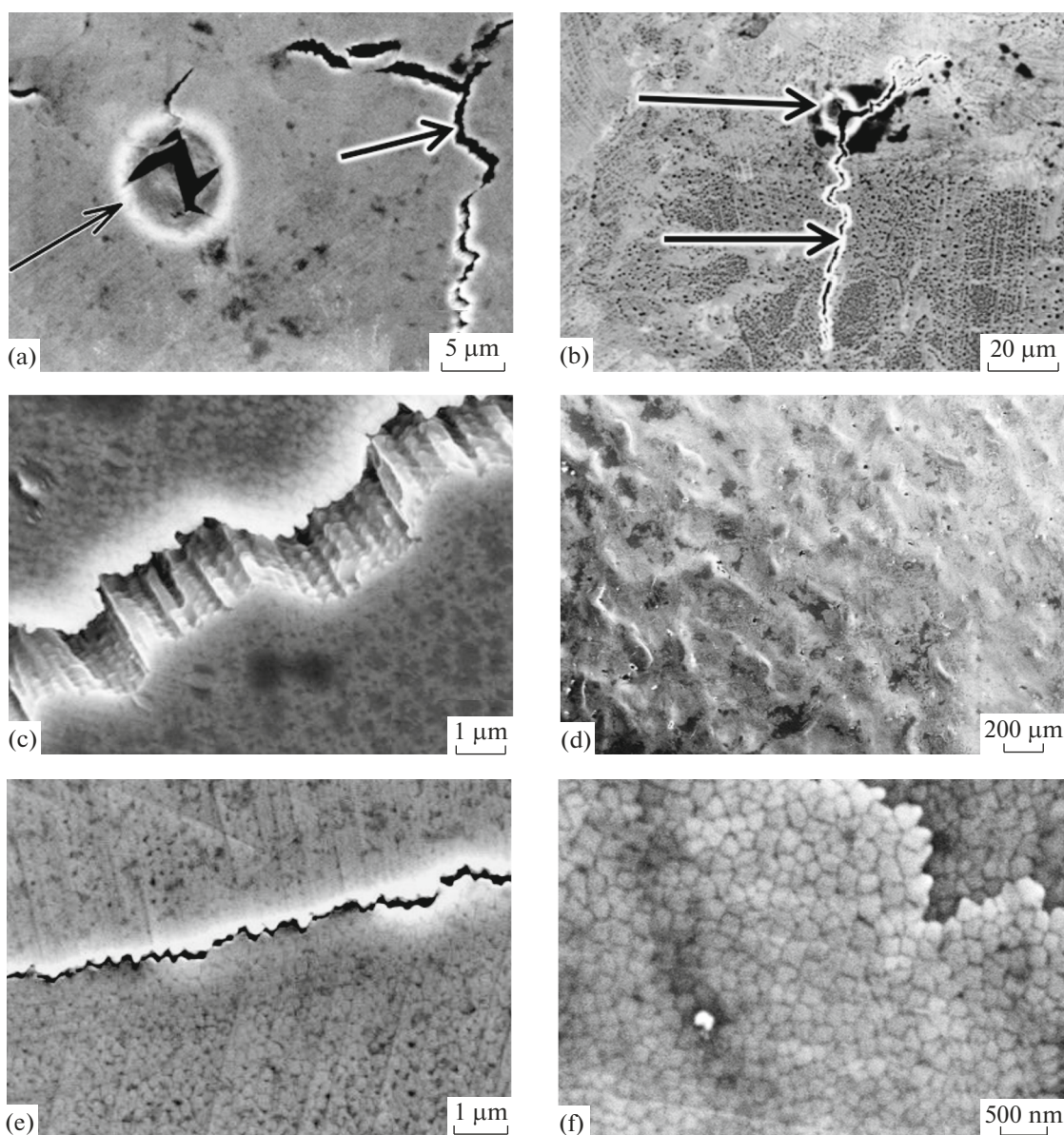


**Fig. 6.** SEM images of the surface of Inconel 718 alloy irradiated with fluxes of helium ions and helium plasma in a hard mode ( $q = 2 \times 10^9 \text{ W/cm}^2$ ,  $\tau = 25 \text{ ns}$ ) at  $N = 10$  (a, b, c) and  $N = 20$  (d, e, f). Blisters with a destroyed shell and microcracks are visible (a, b).

Focus installation with deuterium ion flows and deuterium plasma under similar conditions [28], and is close to the intensity of Nb erosion ( $h \approx 0.05\text{--}0.1 \mu\text{m/pulse}$ ) under the influence of helium ions (HIs) and helium plasma (HP) flows [23].

Numerical modeling of the thermal effect of a fast ion beam on the alloy under study was carried out using the technique proposed for Nb in [23]. A one-dimensional thermal conductivity equation has been solved taking into account the ion beam energy absorption and losses due to thermal radiation in the form of surface Stefan–Boltzmann radiation  $\sigma T^4$ . The

range of fast helium ions in the Inconel 718 alloy is  $d \approx 0.5 \mu\text{m}$  [29]; the other physical characteristics of the material are taken from [27]. In the calculations, it was assumed that the speed of fast ions is  $v \approx 2 \times 10^8 \text{ cm/s}$ , the energy spread is 50–200 keV, the flight path of ions from the anode to the target sample is 8 cm, and the duration of exposure of the ion beam to the alloy is  $t \sim 30\text{--}50 \text{ ns}$ . The energy load on the target in its central part is  $10 \text{ J/cm}^2$  and is determined mainly by fast ions, the energy flux density of which is  $q \sim (2\text{--}3) \times 10^8 \text{ W/cm}^2$ . The pulse shape of the ion beam was specified as a



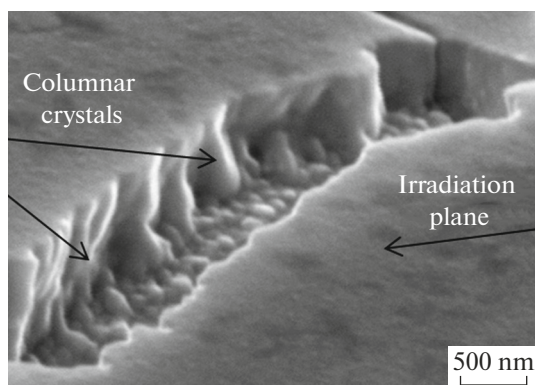


**Fig. 7.** SEM image of the internal sections of a crack in the Nb surface layer irradiated with fluxes of helium ions and helium plasma at  $q = 10^7\text{--}10^8$  W/cm<sup>2</sup>,  $N = 16$  [23]. Columnar crystals are visible, located normal to the irradiation plane.

half-sine wave  $q(t) = q_0 \sin(\pi t/\tau)$  [30]. The results of numerical simulation are given in Table 2.

The calculated data on the evaporated layer thickness  $L_{\text{evap}}$  are in satisfactory agreement with the experimental values, but are somewhat overestimated. This is due to the fact that the calculations did not take into account the above-mentioned possibility of deposition of elements of functional materials onto the target sample.

The calculations performed showed that, in a more severe irradiation mode, the ratio of thicknesses of the melted and evaporated layers per pulse changes significantly: in the soft mode,  $L_{\text{melt}}/L_{\text{evap}} = 8$ , and in the hard mode,  $L_{\text{melt}}/L_{\text{evap}} = 3$ , which means a redistribution of energy absorbed by the alloy during beam-plasma exposure irradiation—with an increase in the power density of radiation incident on the target sample, the share of energy spent on the surface erosion of the material increases, and the share of energy spent on melting the surface layer decreases.

## CONCLUSIONS

Irradiation of the surface layer of Inconel 718 alloy by repeated pulsed exposure to flows of helium ions and helium plasma under two irradiation modes showed that, in each irradiation mode, the processes of sputtering and evaporation of the surface layer of the alloy occurred, as well as its melting and crystallization of the melt at a high rate, affecting the original flat surface morphology of the alloy sample. A wavy relief was observed, containing a thin wrinkled film in the form of ripples in some sites. In the soft irradiation mode, pores were noted on the surface layer microstructure, and with more severe energy impacts, surface microcracks and blisters with destroyed shells also appeared. A cellular microstructure formation in the surface layer was noted, representing a set of flat parallel layers consisting of small cells  $\sim 200$  nm in size.

With an increase in the incident radiation power density, the surface layer erosion intensity increases, but with an increase in the number of pulses to 20 at a fixed value of  $q$  in both irradiation modes, a decrease in the erosion rate is observed, more noticeable in the soft irradiation mode, which is associated with the gradual cleaning of the alloy surface layer from impurity elements absorbed from the environment before irradiation, as well as with the deposition of elements from the composition of functional materials of the working chamber onto the irradiated surface.

An analysis of the thermal effect of a beam of fast ions on the alloy using the method of numerical modeling showed that, with an increase in the value of  $q$ , a redistribution of the shares of energy absorbed by the material occurs, spent on evaporation and melting of the irradiated surface layer, which contributes to increased surface erosion of the material and a decrease in the resulting thickness of the liquid phase.

**Table 2.** Results of calculations by numerical simulation

Energy flux density, $q_0$ , W/cm <sup>2</sup>	$2 \times 10^8$	$1.5 \times 10^9$
Duration of ion beam exposure, $\tau$ , ns	50	25
Distance from anode to target, $L$ , cm	8	4
Maximum temperature of secondary target plasma at the heating stage, $T$ , °C	$1.3 \times 10^4$	$4.3 \times 10^4$
Thickness of molten target layer, $L_{\text{melt}}$ , $\mu\text{m}$	1.6	1.2
Thickness of evaporated target layer, $L_{\text{evap}}$ , $\mu\text{m}$ (calculation)	0.2	0.4
Thickness of evaporated target layer, $L_{\text{evap}}$ , $\mu\text{m}$ (experiment)	0,13	0.27

## FUNDING

This work was carried out under State Assignment no. 075-00715-22-00 and supported by the International Atomic Energy Agency (IAEA CRP grants no. 23664 and no. 24080).

## CONFLICT OF INTEREST

The authors of this work declare that they have no conflicts of interest.

## REFERENCES

- Fridlyander, I.N., *Mashinostroenie. Entsiklopediya*, tom II-3: *Tsvetnye metally i splavy. Kompozitsionnye metallicheskie materialy* (Mechanical Engineering. Encyclopedia, vol. II-3: Non-Ferrous Metals and Alloys. Composite Metal Materials), Moscow: Mashinostroenie, 2001.
- Kablov, E.N. and Golubovskii, E.R., *Zharoprochnost' nikelovykh splavov* (Heat-Resistance of Nickel Alloys), Moscow: Mashinostroenie, 1998.
- Babentsova, L.P. and Antsiferova, I.V., The mechanical properties of the In718 alloy under static and cyclic deformation, *Sovrem. Naukoemkie Tekhnol.*, 2019, no. 6, pp. 14–19.
- Khar'kov, A.A., Shakhmatov, A.V., Gyulikhandanov, E.L., and Alekseeva, E.L., Comparative analysis of corrosion-resistant alloys Inconel 718 and ÉP718, *Chem. Pet. Eng.*, 2019, vol. 54, nos. 8–9, pp. 771–778. <https://doi.org/10.1007/s10556-019-00546-4>
- Konobeev, Yu.V. and Birzhevoi, G.A., Prospects for using high-nickel alloys in power reactors with supercritical-pressure water, *At. Energy*, 2004, vol. 96, no. 5, pp. 365–373. <https://doi.org/10.1023/B:ATEN.0000038104.58523.cd>
- Cherepanov, A.N. and Ovcharenko, V.E., Effect of nanostructured composite powders on the structure and strength properties of the high-temperature Inconel 718 alloy, *Phys. Met. Metallogr.*, 2015, vol. 116, no. 12, pp. 1279–1284. <https://doi.org/10.1134/S0031918X1510004X>
- Budilov, V.V., Ivanov, V.Yu., and Mukhin, V.S., *Integrirovannye vakuurnye ionno-plazmennye tekhnologii obrabotki detalei GTD. Fizicheskie osnovy, modelirovanie, proektirovanie* (Integrated Vacuum Ion-Plasma Technologies of GTE Parts Processing. Physical Foundations, Modeling, Design), Ufa: Gilem, 2004.
- Litye lopatki gazoturbinnnykh dvigatelei: Splavy, tekhnologii, pokrytiya* (Cast Blades of Gas Turbine Engines: Alloys, Technologies, Coatings), Kablov, E.N., Ed., Moscow: Nauka, 2006.
- Smyslov, A.M., Mingazhev, A.D., Selivanov, K.S., Smyslova, M.K., and Mingazheva, A.A., Ion-plasma technology of coating formation on blades GTE turbine blades made of heat-resistant nickel alloys, *Vestn. Ufimsk. Gos. Aviats. Tekh. Univ.*, 2012, vol. 16, no. 1 (46), pp. 77–80.
- Kablov, E.N. and Muboyadzhyan, S.A., Heat-resistant and heat-protective coatings for high-pressure turbine blades of promising GTE, *Aviats. Mater. Tekhnol.*, 2012, no. 5, pp. 60–70.
- Zlenko, M.A., Popovich, A.A., and Mutyulina, I.N., *Additivnye tekhnologii v mashinostroenii* (Additive Technologies in Mechanical Engineering), St. Petersburg: S.-Peterb. Gos. Politekh. Univ., 2013.
- Shamsaei, N., Yadollahi, A., Bian, L., and Thompson, S.M., An overview of direct laser deposition for additive manufacturing. Part I: Transport phenomena, modeling and diagnostics, *Addit. Manuf.*, 2015, vol. 8, pp. 36–62. <https://doi.org/10.1016/j.addma.2015.07.001>
- Shamsaei, N., Yadollahi, A., Bian, L., and Thompson, S.M., An overview of direct laser deposition for additive manufacturing. Part II: Mechanical behavior, process parameter optimization and control, *Addit. Manuf.*, 2015, vol. 8, pp. 12–35. <https://doi.org/10.1016/j.addma.2015.07.002>
- Debroy, T., Wei, H.L., Zuback, J.S., and Mukherjee, T., Additive manufacturing of metallic components—process, structure and properties, *Prog. Mater. Sci.*, 2018, vol. 92, pp. 112–224. <https://doi.org/10.1016/j.pmatsci.2017.10.001>
- Ngo, T.D., Kashani, A., Imbalzano, G., and Nguyen, K.T.Q., Additive manufacturing (3D printing): A review of materials, methods, applications and challenges, *Composites, Part B*, 2018, vol. 143, pp. 172–196. <https://doi.org/10.1016/j.compositesb.2018.02.012>
- Gryaznov, M.Yu., Shotin, S.V., and Chuvil'deev, V.N., Physico-mechanical properties and structure of Inconel 718 alloy obtained by selective laser melting technology, *Vestn. Nizhegorodsk. Univ. im. N.I. Lobachevskogo*, 2014, no. 4 (1), pp. 46–51.
- Rashkovets, M.V., Nikulina, A.A., Klimova-Korsmik, O.G., Babkin, K.D., Matts, O.E., and Mazzarisi, M., The phase composition of the nickel-based Inconel 718 alloy obtained by additive technology, *Obrab. Met. (Tekhnol., Oborud., Instrum.)*, 2020, vol. 22, no. 3, pp. 69–81. <https://doi.org/10.17212/1994-6309-2020-22.3-69-81>
- Rashkovets, M.V., Kislov, N.G., Nikulina, A.A., and Klimova-Korsmik, O.G., Effect of heat treatment on the structure, phase composition and impact toughness of Inconel 718 alloy under additive manufacturing, *Photonics Russ.*, 2021, vol. 15, no. 7, pp. 568–575. <https://doi.org/10.22184/1993-7296.FRos.2021.15.7.568.575>
- Borovitskaya, I.V., Gribkov, V.A., Grigorovich, K.V., Demin, A.S., Maslyaev, S.A., Morozov, E.V., Pimenov, V.N., Sprygin, G.S., Zepelev, A.B., Gusakov, M.S., Logachev, I.A., Bondarenko, G.G., and Gaidar, A.I., Effect of pulsed helium ion fluxes and helium plasma on the Inconel 718 alloy, *Russ. Metall. (Metally)*, 2018, vol. 2018, no. 9, pp. 826–834. <https://doi.org/10.1134/S0036029518090057>
- Gribkov, V.A., Demin, A.S., Demina, E.V., Dubrovskii, A.V., Karpinskii, L., Maslyaev, S.A., Padukh, M., Pimenov, V.N., and Sholz, M., Physical processes of interaction between ion and plasma streams and a target surface in the Dense Plasma Focus device, *Prikl. Fiz.*, 2011, no. 3, pp. 43–51. <https://ap-physics.orion-ir.ru/appl-11/11-3/PF-11-3-43.pdf>

21. Bondarenko, G.G., Kabanova, T.A., and Rybalko, V.V., *Osnovy materialovedeniya* (Fundamentals of Material Science), Bondarenko, G.G., Ed., Moscow: Binom. Laboratoriya Znaniy, 2014.
22. Pimenov, V.N., Borovitskaya, I.V., Gribkov, V.A., Demin, A.S., Epifanov, N.A., Maslyaev, S.A., Morozov, E.V., Sasinovskaya, I.P., Bondarenko, G.G., Gaydar, A.I., and Paduch, M., Influence of pulsed flows of deuterium ions and deuterium plasma on Cu–Ni and Cu–Ni–Ga alloys, *J. Surf. Invest.: X-Ray, Synchrotron Neutron Tech.*, 2022, vol. 16, no. 1, pp. 33–41. <https://doi.org/10.1134/S1027451022010153>
23. Pimenov, V.N., Borovitskaya, I.V., Demin, A.S., Epifanov, N.A., Latyshev, S.V., Maslyaev, S.A., Morozov, E.V., Sasinovskaya, I.P., Bondarenko, G.G., and Gaidar, A.I., Damage of niobium by pulsed flows of helium ions and helium plasma, *Inorg. Mater.: Appl. Res.*, 2022, vol. 13, no. 3, pp. 687–695. <https://doi.org/10.1134/S2075113322030303>
24. Novikov, I.I., *Teoriya termicheskoi obrabotki metallov* (Theory of Thermal Treatment of Metals), Moscow: Metallurgiya, 1986.
25. Demin, A.S., Maslyaev, S.A., Pimenov, V.N., Gribkov, V.A., Demina, E.V., Latyshev, S.V., Lyakhovitskii, M.M., Sasinovskaya, I.P., Bondarenko, G.G., Gaidar, A.I., and Padukh, M., Exposure of powerful pulsed flows of deuterium ions and deuterium plasma on a molybdenum plate, *Fiz. Khim. Obrab. Mater.*, 2017, no. 6, pp. 5–17.
26. Borovitskaya, I.V., Nikulin, V.Ya., Bondarenko, G.G., Mikhailova, A.B., Silin, P.V., Gaidar, A.I., Paramonova, V.V., and Peregudova, E.N., Effect of pulsed nitrogen plasma and nitrogen ion fluxes on the structure and mechanical properties of vanadium, *Russ. Metall. (Metally)*, 2018, vol. 2018, no. 2, pp. 266–275. <https://doi.org/10.1134/S0036029518030023>
27. Agazhanov, A., Samoshkin, D., and Kozlovskii, Yu., Thermophysical properties of Inconel 718 alloy, *J. Phys.: Conf. Ser.*, 2019, vol. 1382, no. 1, p. 012175. <https://doi.org/10.1088/1742-6596/1382/1/012175>
28. Pimenov, V.N., Maslyaev, S.A., Demina, E.V., Kovtun, A.V., Sasinovskaya, I.P., Gribkov, V.A., and Dubrovskii, A.V., Interaction of powerful pulsed energy flows with the tungsten surface in the device Plasma Focus, *Fiz. Khim. Obrab. Mater.*, 2008, no. 3, pp. 5–14.
29. *Handbook of Physical Quantities*, Grigoriev, I.S. and Meilikhov, E.Z., Eds., Boca Raton: CRC Press, 1996.
30. Gribkov, V.A., Latyshev, S.V., Maslyaev, S.A., and Pimenov, V.N., Numerical simulation of the pulsed energy flows interaction with material in the devices Plasma Focus, *Fiz. Khim. Obrab. Mater.*, 2011, no. 6, pp. 16–22.

*Translated by V. Selikhanovich*

**Publisher's Note.** Pleiades Publishing remains neutral with regard to jurisdictional claims in published maps and institutional affiliations.